



Figures and figure supplements

Motoneuron Wnts regulate neuromuscular junction development

Chengyong Shen et al

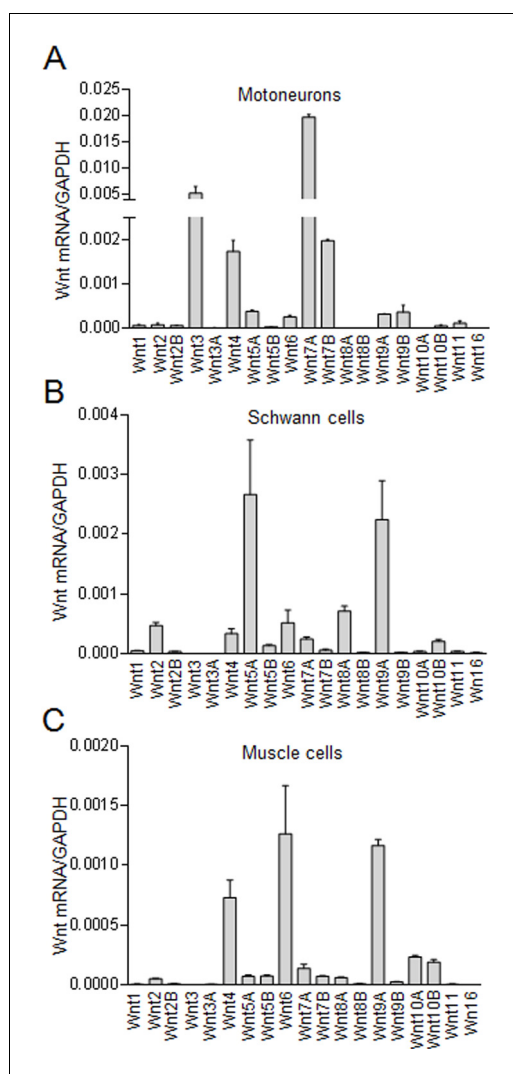


Figure 1. Wnt expression in motoneurons, Schwann cells, and muscle cells. (A) Wnt expression in motoneurons. Motoneurons in HB9-tdTomato mice (P0) were isolated by FACS. mRNAs were subjected to real-time PCR with GAPDH as internal control. (B) Wnt expression in primary Schwann cells. Sciatic nerves were isolated from P3 mice for primary Schwann cell culture. mRNAs were subjected to real-time PCR with GAPDH as internal control. (C) Wnt expression in C2C12 muscle cells. mRNAs were isolated from C2C12 myotubes and subjected to real-time PCR with GAPDH as internal control.

DOI: <https://doi.org/10.7554/eLife.34625.002>

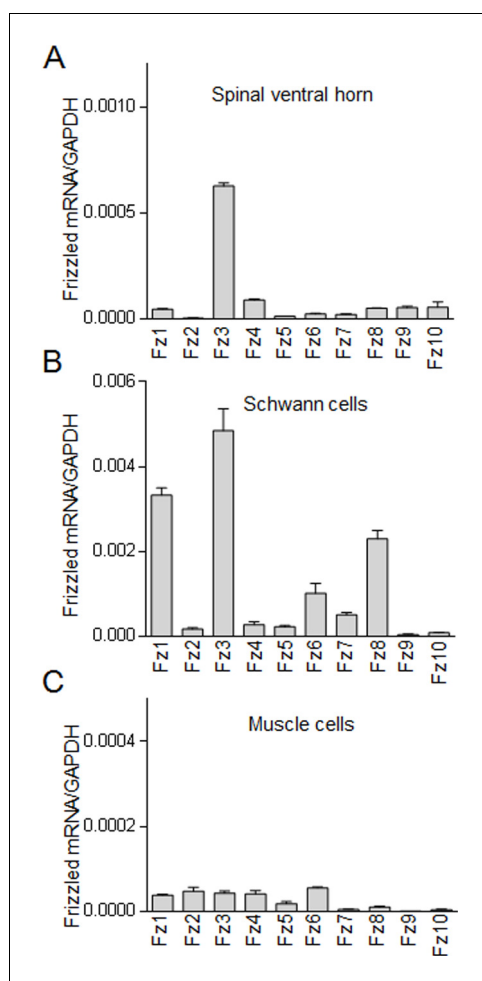


Figure 1—figure supplement 1. Frizzled expression in spinal ventral horn, Schwann cells, and muscle cells. (A) Expression of Frizzled mRNA in spinal ventral cord. ChAT-EGFP mice were dissected to separate the spinal ventral horn. mRNA was subjected for real-time PCR analysis of Frizzled expression. GAPDH was set as internal control. (B) Expression of Frizzled mRNA in primary Schwann cells. Sciatic nerve in wide type mice (P3) was isolated and dissociated for primary Schwann cells culture, and their mRNA were subjected for real-time PCR analysis. GAPDH was set as internal control. (C) Expression of Frizzled mRNA in muscle cells. C2C12 myoblast was fused into myotubes and their mRNA was subjected for real-time PCR analysis. GAPDH was set as internal control.

DOI: <https://doi.org/10.7554/eLife.34625.003>

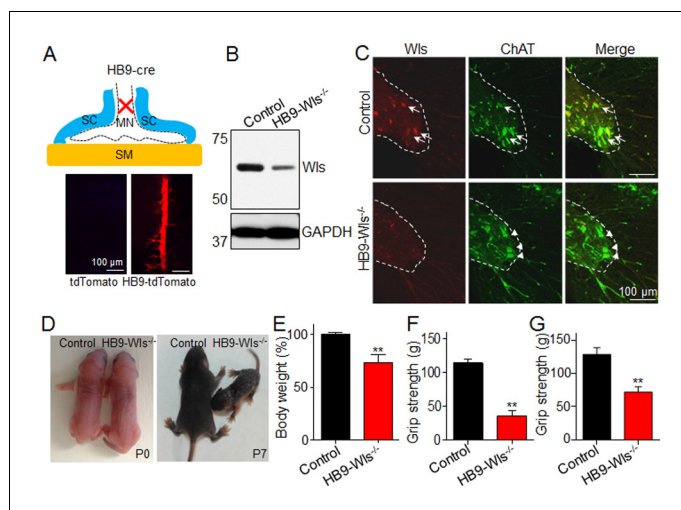


Figure 2. Ablation of Wls expression in motoneuron causes muscle weakness. (A) Up: NMJ structure. Cre targets motoneuron (HB9::cre). Down: Cre expression was verified by crossing HB9::cre mice with Rosa-tdTomato reporter mice (HB9-tdTomato). HB9::cre drives tdTomato expression in the middle line of diaphragm where motoneuron innervates in the muscle (HB9-tdTomato, (P7). MN, motoneuron; SC, Schwann cells; SM, skeletal muscle. (B) Immunoblot of Wls in sciatic nerve from 2-month-old control and HB9-Wls^{-/-} mutant. Notice that the reduced Wls protein expression in the mutant. (C) Immunostaining of Wls in spinal cord from 2-month-old control and HB9-Wls^{-/-} mutant. Notice that Wls staining signal is lost in the ChAT positive cells in the spinal ventral horn in the HB9-Wls^{-/-}. Anti-Wls (Red); Anti-ChAT (Green). Arrows indicate colocalization of Wls and ChAT protein. (D) Two genotypes at P0 and P7. Notice that apparent normal size at P0, and reduced body size at P7. (E) Body weight of two genotypes at P7. Control, n = 20; mutant, n = 11; Unpaired t-test, **p<0.01. (F) Grip strength of two genotypes at P60. Control, n = 5; mutant, n = 5. Unpaired t-test, **p<0.01. (G) Grip strength of two genotypes with same body weight at P60. Control, n = 5; mutant, n = 5. Unpaired t-test, **p<0.01.

DOI: <https://doi.org/10.7554/eLife.34625.004>

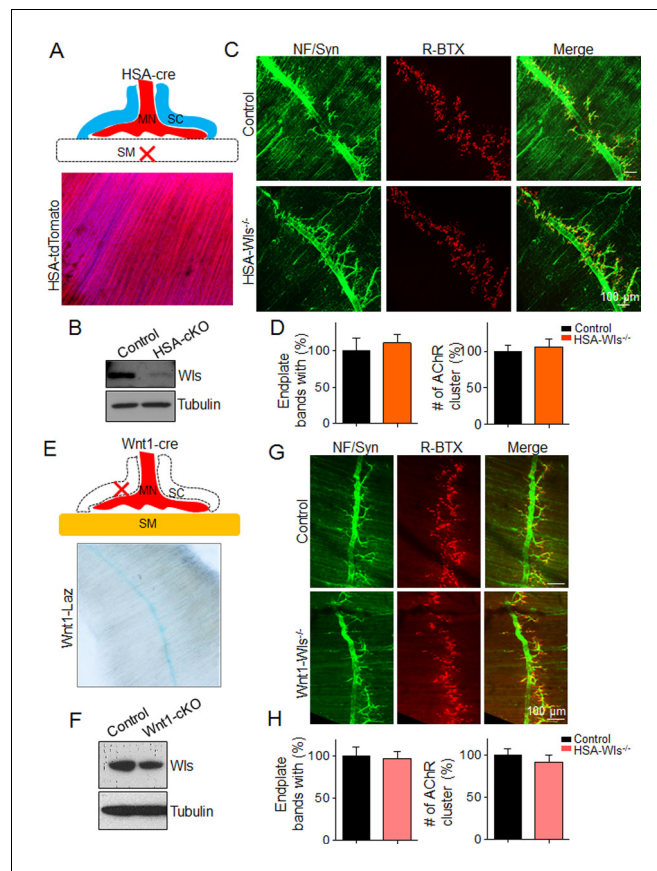


Figure 2—figure supplement 1. Ablation of WIs in skeletal muscle or Schwann cell has no apparent NMJ morphological defects. (A) Up: NMJ structure. Cre targets skeletal muscle (HSA::cre). Down: Cre expression was verified by crossing HSA::cre mice with Rosa-tdTomato reporter mice (HSA-tdTomato, (P7). HSA::cre drives tdTomato protein expression in each muscle fiber of diaphragm. (B) Immunoblot of WIs protein in gastrocnemius of P5 control and HSA-WIs^{-/-} mice. (C) Immunostaining of NMJs in diaphragms of P5 control and HSA-WIs^{-/-} mice with anti-NF and anti-Syn (Green). R-BTX stains postsynaptic AChR (Red). Control: Cre or WIs^{+/+} littermates. (D) Statistical results of endplate width (Left), AChR number (Right) in B. n = 5 mice per group; Unpaired t-test. p>0.05. (E) Up: NMJ structure. Cre targets Schwann cells (Wnt1::cre). Down: Cre expression was verified by crossing Wnt1::cre mice with Rosa-Laz reporter mice (Wnt1-Laz, (P7). Wnt1::cre drives laz expression in middle line of diaphragm where Schwann cells surround the innervated motor axons (Wnt1-Laz). (F) Immunoblot of WIs protein in sciatic nerve of E18.5 control and Wnt1-WIs^{-/-} mice. (G) Immunostaining of NMJs in diaphragms of E18.5 control and Wnt1-WIs^{-/-} with anti-NF and anti-Syn (Green), R-BTX (Red). Control: Cre or WIs^{+/+} littermates. (H) The statistics of endplate width (Left), AChR number (Right) in E. n = 5 mice per group; Unpaired t-test. p>0.05.

DOI: <https://doi.org/10.7554/eLife.34625.005>

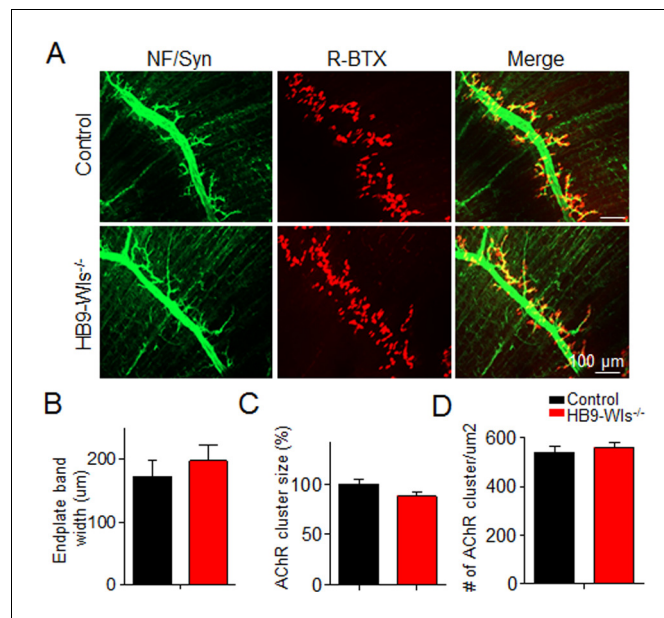


Figure 2—figure supplement 2. NMJ formation appears grossly normal in HB9-Wls^{-/-} mice. (A) Immunostaining of NMJs in diaphragm of E18.5 control and HB9-Wls^{-/-} embryos with anti-NF and anti-Syn to label motoneuron axons and synaptic vesicles (Green). R-BTX stains postsynaptic AChR (Red). (B) Statistical results of endplate band width of two genotypes. $n = 3$ mice per group; Unpaired t-test, $p > 0.05$. (C) Statistical results of AChR cluster size. $n = 3$ mice per group; Unpaired t-test, $p > 0.05$. (D) Statistical results of AChR number. $n = 3$ mice per group; Unpaired t-test, $p > 0.05$.

DOI: <https://doi.org/10.7554/eLife.34625.006>

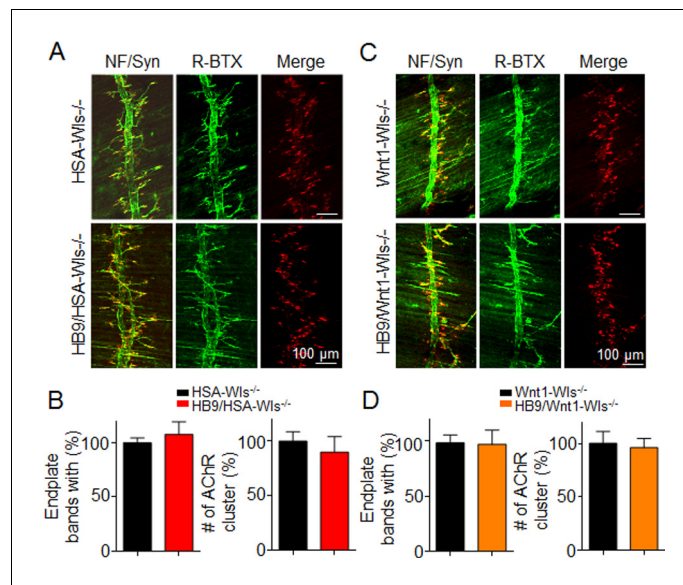


Figure 2—figure supplement 3. Comparable NMJ formation between HSA-Wls^{-/-} and HB9/HSA-Wls^{-/-}, Wnt1-Wls^{-/-} and HB9/Wnt1-Wls^{-/-} mice. (A) Immunostaining of NMJs in diaphragms of HSA-Wls^{-/-} and HB9/HSA-Wls^{-/-} E18.5 embryos with anti-NF/Syn (Green). R-BTX stains postsynaptic AChR (Red). Scale bar, 100 μ m. (B) The statistics of endplate width and AChR cluster number in A. n = 3 mice per group; Unpaired t-test. p>0.05. (C) Immunostaining of NMJs in diaphragms of Wnt1-Wls^{-/-} and HB9/Wnt1-Wls^{-/-} E18.5 embryos with anti-NF/Syn (Green). R-BTX stains postsynaptic AChR (Red). Scale bar, 100 μ m. (D) The statistics of endplate width and AChR cluster number in C. n = 3 mice per group; Unpaired t-test. p>0.05.

DOI: <https://doi.org/10.7554/eLife.34625.007>

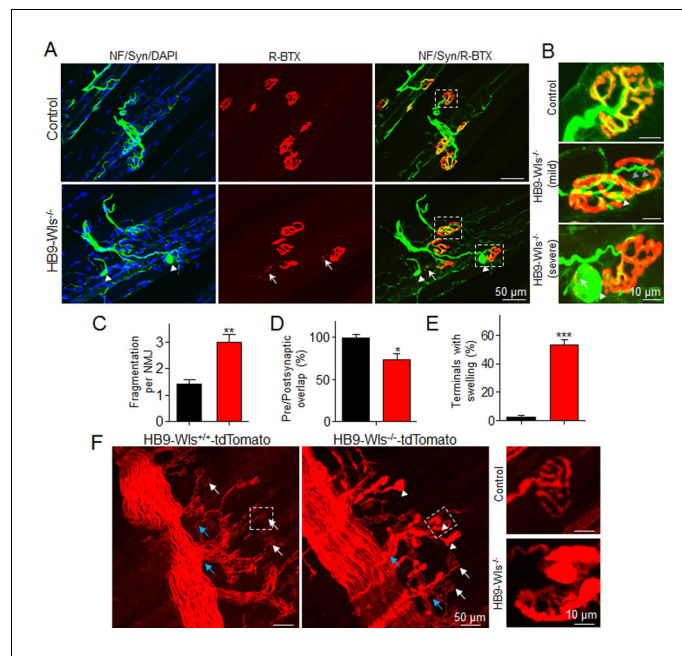


Figure 3. Abnormal pre- and postsynaptic NMJ structure in HB9-Wls^{-/-} mutant mice. (A) Immunostaining of NMJs in gastrocnemius of 2-month-old control and HB9-Wls^{-/-} mice with anti-NF/anti-Syn (Green) and R-BTX (Red). Nuclei were labeled with DAPI (Blue). In mutant, some nerve terminals are swollen (white arrowhead) and AChR clusters are broken (white arrow). (B) The high magnification of boxed area in A. White arrowhead indicates swollen nerve terminals. Blue arrowhead indicates motor nerve detaching from AChR clusters; White arrow indicates broken pieces of AChR. (C) Statistical results of AChR fragmentation per NMJ. $n = 3$ mice per group; Unpaired t-test, $**p < 0.01$. (D) Percentage of AChR cluster innervated with nerve terminals. $n = 3$ mice per group; Unpaired t-test, $*p < 0.05$. (E) Percentage of nerve terminal swellings. $n = 3$ mice per group; Unpaired t-test, $***p < 0.001$. (F) The diaphragm of 2-month-old HB9-tdTomato and HB9-WLS^{-/-} tdTomato mice. Nerve terminal swellings are indicated with white arrowhead. Normal nerve terminals are indicated with white arrow. Axon branch are indicated with blue arrow. Boxes indicated by dash line were enlarged in the right.

DOI: <https://doi.org/10.7554/eLife.34625.008>

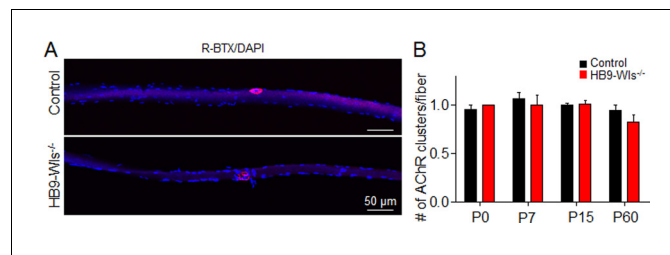


Figure 3—figure supplement 1. Wls loss in motoneuron does not enhance synapse number in single muscle fiber. (A) Representative images of individual gastrocnemius muscle fibers of 2-month-old control and HB9-Wls^{-/-} mice. To visualize AChR clusters on single muscle fibers, gastrocnemius was fixed in 4% PFA and stained with R-BTX (Red) and DAPI (Blue) to show AChR clusters and myonuclei. Muscles were washed three times in PBS and teased into single fibers and mounted in Vectashield mounting medium. We counted the number of AChR cluster in each single muscle fiber and defined that synapse elimination was impaired when more than one AChR cluster was found after P15. (B) Quantitative analysis of NMJ number per muscle fiber. NMJ number per muscle fiber was comparable between control and HB9-Wls^{-/-} mice at P0, P7, P15, and P60. n = 3 mice per group. Unpaired t-test, p>0.05.

DOI: <https://doi.org/10.7554/eLife.34625.009>

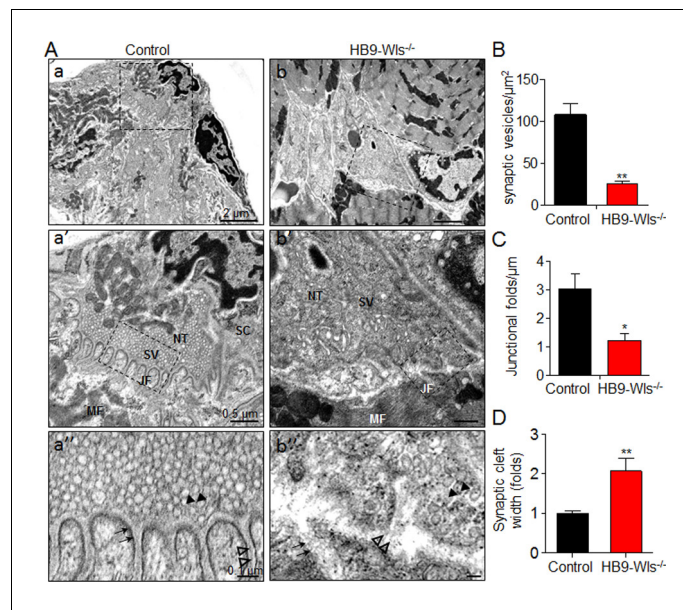


Figure 4. Disruption of NMJ ultrastructure in HB9-Wls^{-/-} mutant mice. (A) Representative EM images of diaphragm NMJs in P15 control (a, a', a'') and HB9-Wls^{-/-} mice (b, b', b''). Notice that there is a dramatic reduction of synaptic vesicles number in the HB9-Wls^{-/-} (black arrowhead, (a'' and b'')) and loss of synaptic junctional folds (black arrow, (a'' and b'')) and basal lamina (empty arrowhead, (a'' and b'')) in HB9-Wls^{-/-}. Boxed regions are shown at higher magnification immediately below. NT, nerve terminal; MF, muscle fiber; SC, Schwann cell; SV, synaptic vesicle; JF, junctional fold. Scale bars: 2.0 μ m (top); 0.5 μ m (middle); 0.1 μ m (bottom). (B) Synaptic vesicle density in two genotypes. n = 3 mice per group; Unpaired t-test, **p<0.01. (C) Number of synaptic junctional folds. n = 3 mice per group; Unpaired t-test, *p<0.05. (D) Synaptic cleft width. n = 3 mice per group; Unpaired t-test, **p<0.01. DOI: <https://doi.org/10.7554/eLife.34625.010>

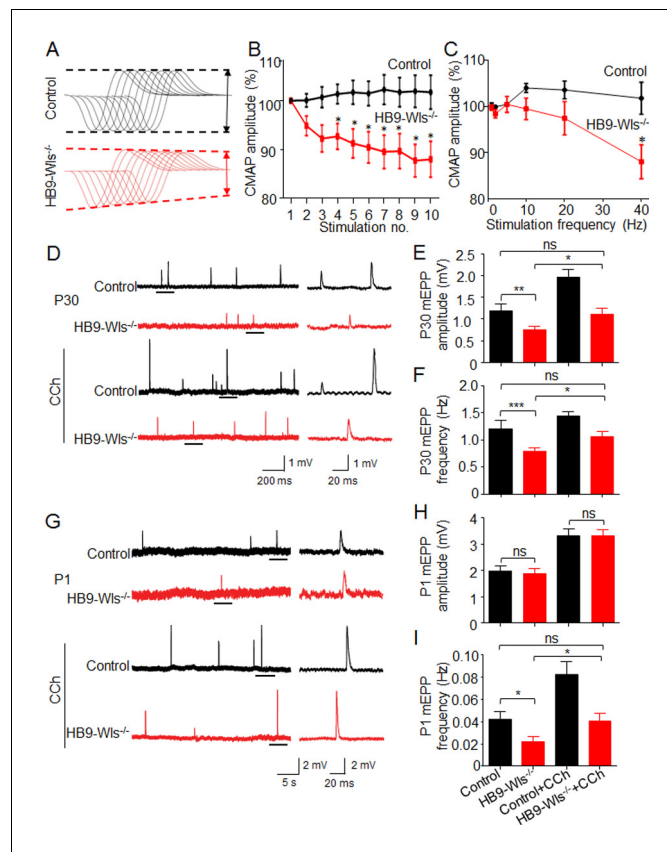


Figure 5. Wls loss in motoneuron impairs neurotransmission initially from presynapse. (A) CMAPs were recorded in gastrocnemius from P30 mice in response to a train of 10 submaximal stimuli at different frequencies. The first stimulus response in control mice was designated as 100%. Representative 10 CMAP traces, shown stacked in succession for better comparison. (B) Reduced CMAP amplitudes at 40 Hz in HB9-Wls^{-/-} mice. $n = 4$ mice per group. Two-way ANOVA, $*p < 0.05$. (C) CMAP amplitudes of the tenth stimulation at different stimulation frequencies. $n = 4$ mice per group. Two-way ANOVA, $*p < 0.05$. (D) Representative mEPP traces from P30 mice. mEPPs were recorded from hemidiaphragms. Traces underlined on the left are enlarged on the right. (E) Reduced mEPP amplitudes in mutant mice and CCh effects at P30. $F_{(2, 9)} = 13.56$, ns , $p > 0.05$, $**p < 0.01$. $n = 4$ mice per group, 5–6 muscle fibers per mouse; One-way ANOVA. (F) Reduced mEPP frequencies in mutant mice and CCh effect at P30. $F_{(2, 9)} = 14.2$, ns , $p > 0.05$, $**p < 0.01$, $*p < 0.05$, $n = 4$ mice per group, 5–6 muscle fibers per mouse; One-way ANOVA. (G) Representative mEPP traces from P1 mice. (H) Comparable mEPP amplitude between two genotypes and CCh effect at P1. $F_{(2, 9)} = 63.07$, ns , $p > 0.05$, $***p < 0.001$. $n = 4$ mice per group, 5–6 muscle fibers per mouse; One-way ANOVA. (I) Reduced mEPP frequency in mutant mice and CCh effect at P1. $F_{(2, 9)} = 12.87$, ns , $p > 0.05$, $**p < 0.01$. $n = 4$ mice per group, 5–6 muscle fibers per mouse; One-way ANOVA.

DOI: <https://doi.org/10.7554/eLife.34625.011>

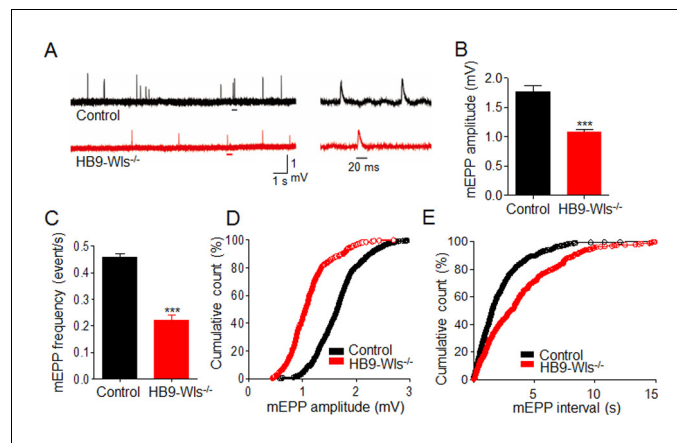


Figure 5—figure supplement 1. Impairment of pre- and postsynaptic prosperity in P15 HB9-Wls^{-/-} mice. (A) Representative mEPP traces from P15 mice. mEPPs were recorded from hemidiaphragms. Traces underlined on the left are enlarged on the right. (B) Reduced mEPP amplitudes in diaphragms of HB9-Wls^{-/-} mice at P15. $n = 4$ mice per group, 5–6 muscle fibers per mouse; Unpaired t-test, *** $p < 0.001$. (C) Reduced mEPP frequencies in diaphragms of HB9-Wls^{-/-} mice at P15. *** $p < 0.001$. $n = 4$ mice per group, 5–6 muscle fibers per mouse; Unpaired t-test, *** $p < 0.001$. (D) Cumulative plots of mEPP events against amplitudes. (E) Cumulative plots of mEPP events against intervals.

DOI: <https://doi.org/10.7554/eLife.34625.012>

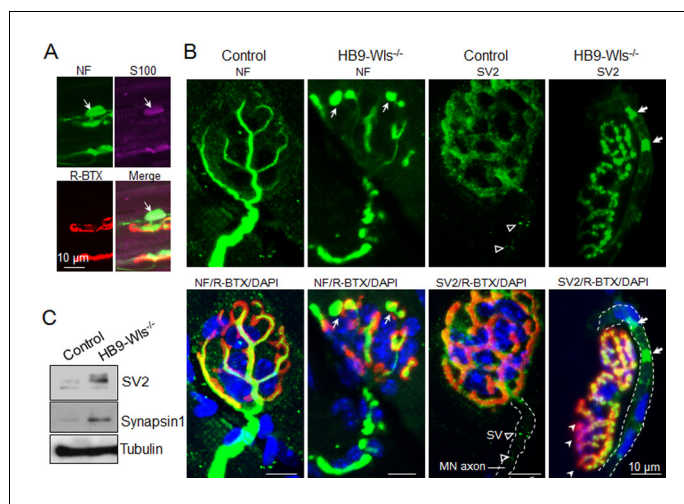


Figure 6. Clustered synaptic vesicles in HB9-Wls^{-/-} axons. (A) Immunostaining of axonal terminal swelling in gastrocnemius of P21 HB9-Wls^{-/-} mice with anti-NF (Green), anti-S100 (Purple), R-BTX (Red). (B) Immunostaining of NMJs in gastrocnemius of 2-month-old control and mutant mice with anti-NF or anti-SV2 to label synaptic vesicles (Green). R-BTX indicates the AChR (Red). Cell nucleus is labeled with DAPI (Blue). Dashed line indicates motor axon. Notice that in the mutant NMJ, there are aberrant deposits of synaptic vesicles in the motor axon (bold white arrow in mutant and empty arrowhead in control), and reduced overlap between pre and post-synapse (white arrowhead). Nucleuses around motor axons are from Schwann cells. (C) Immunoblot of SV2 and Synapsin 1 in phrenic nerve at 2-month-old control and mutant mice.

DOI: <https://doi.org/10.7554/eLife.34625.013>

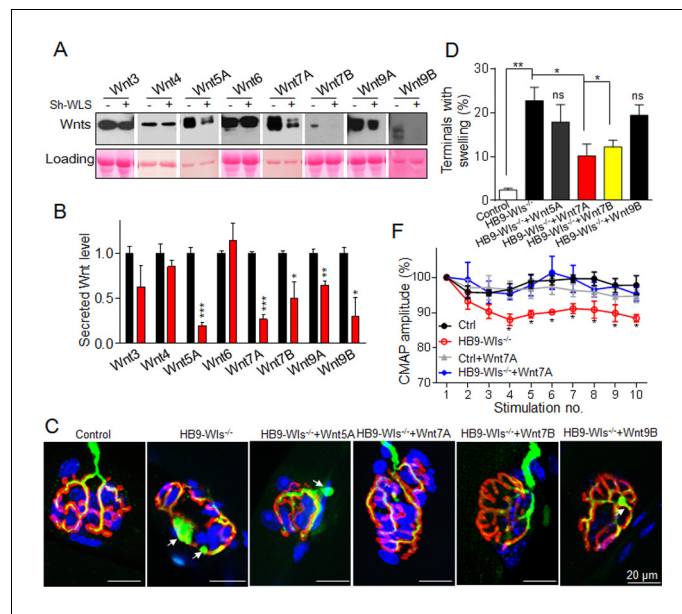


Figure 7. Wnt7A partially rescues axonal terminal swelling in HB9-Wls^{-/-} mice. **(A)** Wls-dependent Wnts secretion. HEK293T cells were co-transfected with shRNA of Wls and motoneuron Wnts cDNA with a Flag tag. Conditioned medium was collected for testing secreted Wnt. Ponceau S red indicates the loading. **(B)** Statistical results of secreted Wnt protein levels in conditioned medium in A. * $p < 0.05$, ** $p < 0.01$, *** $p < 0.001$. Unpaired t-test. Three independent experiments were performed. **(C)** Immunostaining of mutant TA muscles injected with Wnt recombinant proteins. Wnt recombinant proteins (10 ng/ μ l, 20 μ l) were injected into TA muscles of right leg in HB9-Wls^{-/-} mice at every three days. TA muscle of left leg in the same mouse was injected with vesicle as control. Thirty days later, TA muscle was isolated for NMJ staining. Compared with control, Wnt5A or Wnt9B, Wnt7A and Wnt7B partially rescued the axon terminal swelling in HB9-Wls^{-/-} mice. Anti-NF/Syn: Green; R-BTX: Red; DAPI: Blue. **(D)** Statistical results of F. Control group: $n = 5$ mice; HB9-Wls^{-/-} group: $n = 6$ mice; HB9-Wls^{-/-} + Wnt5A group: $n = 6$ mice; HB9-Wls^{-/-} + Wnt7A group: $n = 5$ mice. HB9-Wls^{-/-} + Wnt7B group: $n = 5$ mice. HB9-Wls^{-/-} + Wnt9B group: $n = 5$ mice. Unpaired t-test, * $p < 0.05$, ** $p < 0.01$. ns, non-significant. **(E)** Increased CMAP amplitudes in HB9-Wls^{-/-} mice by Wnt7A at 30 Hz stimulation. Control group: Black; HB9-Wls^{-/-} group: Red; Control +Wnt7A group: Gray; HB9-Wls^{-/-} + Wnt7A group: Blue. $n = 4$ mice per group; Two-way ANOVA, * $p < 0.05$.

DOI: <https://doi.org/10.7554/eLife.34625.014>